ACS Catalysis

pubs.acs.org/acscatalysis Research Article

Photoredox Catalysis: The Reaction Mechanism Can Adjust to Electronic Properties of a Catalyst

Katarzyna Goliszewska, Katarzyna Rybicka-Jasińska, John A. Clark, Valentine I. Vullev,* and Dorota Gryko*

Cite This: *ACS Catal.* 2020, 10, 5920−5927 Read Online

ACCESS | Metrics & More | Article Recommendations | Supporting Information

ABSTRACT: Photochemistry provides paths to reactive intermediates that are often inaccessible by any other means. Most organic molecules, however, are colorless and require photocatalysts absorbing in the visible spectral region for transferring the required energy and charges. The electrochemical potentials of a photocatalyst, along with its optical excitation energy, guide its selection for driving oxidative or reductive reactions. Such selection criteria, however, frequently undermine the complexity of the transformations and prove limiting. Herein, we demonstrate how electron-rich and electron-deficient photoredox catalysts, with distinctly different reduction potentials, successfully drive the same reaction with similarly good yields. The analysis reveals that the large differences between the optical and electrochemical frontier-orbital energy gaps cause switching between two parallel reaction pathways—oxidative versus reductive quenching. This finding demonstrates a paradigm where reaction mechanism adjusts to the electronic properties of catalysts and opens doors for diversifying and broadening of the applicability of photochemical transformations.

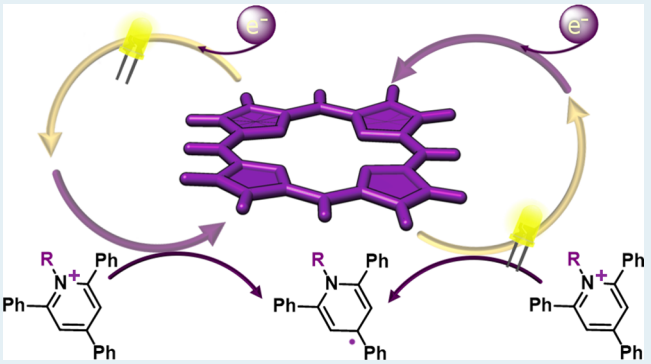

KEYWORDS: *photochemistry, photoredox catalysis, porphyrins, pyridinium salts, mechanistic studies*

INTRODUCTION

In the recent years, the renaissance of photochemistry has made it one of the most dynamically growing branches of organic chemistry. Encompassing endergonic reactions where light can be viewed as a "reagent" driving the transformations,[1−3] the field of photocatalysis offers considerably more than what "classic" catalysis does. Currently, dyes that utilize absorbed light energy to drive endergonic chemical transformations, via turnover cycling between ground and excited states, are the focus of one of the fastest growing branches of photocatalysis.[4,5] The IUPAC recommendations from the mid-2000s appear to reflect this important trend by removing the limitation for exergonicity from the definition of "photocatalysis".[1]

Activation of organic molecules, mediated by visible light, enables a large number of organic transformations including oxidations,[6−8] reductions,[9] formation of carbon−carbon[10−12] and carbon−heteroatom[13,14] bonds, and functionalization of inactivated C−H bonds.[15,16] It is possible to sustain the pace of breakthroughs in this field, however, only if deepening the mechanistic understanding of light driven reactions accompanies the development of new synthetic methods in order to fill the growing gap between utilitarian experimental results and pursuits of fundamental knowledge.[17−19]

In the early years of photoredox chemistry, serendipity and empirical deductions drove the selection of photocatalysts (PCs). Nowadays, on the other hand, the relationships between the electrochemical and optical properties of catalysts and substrates typically defines the basis for choosing an optimal PC. Previous reports provide guidelines how to control the oxidizing and reducing propensities of both transition-metal based[20−22] and organic PCs.[23−25] Depending on its electrochemical properties, the photoexcited catalyst, PC*, undergoes photoinduced-charge-transfer (PCT) with an electron donor or acceptor, initiating a turnover cycle via reductive or oxidative quenching, respectively.[4]

As discussed in recent years, chemical transformations can proceed via oxidative and reductive quenching cycles depending on reaction settings such as the type of PC and redox-active substrates present.[4,5] Stephenson et al. report efficient switching between oxidative and reductive pathways in protocols for photoinduced atom-transfer radical addition

Received: January 13, 2020
Revised: April 23, 2020
Published: April 28, 2020

https://dx.doi.org/10.1021/acscatal.0c00200
ACS Catal. 2020, 10, 5920−5927

(ATRA) catalyzed by $[Ir\{dF(CF_3)ppy\}_2(dtbbpy)]PF_6$ (oxidative quenching) or $[Ru(bpy)_3]Cl_2$ (reductive quenching).[26,27] Similarly, both quenching manifolds can lead to photocatalytic activation of *N*-(acyloxy)-phthalimides (NHPI esters), popular sources of alkyl radicals, depending on the nature of a PC.[28,29] Active promoting of one mechanistic pathway often affects the overall result by, e.g., suppressing side reactions or broadening applicability of the process.[26] In exceptional cases, catalyst-controlled divergent catalytic cycles allow for the formation of different products as in the fragmentation of *N*-acyl-isoxazol-5-ones reported by Zhou et al.[30] Is it always necessary, however, to actively control the exact reaction pathways by selecting PCs with specific electronic properties? May we, under exactly the same conditions, obtain similar results and switch between alternative mechanisms, and even more, have these two mechanism operate in parallel? What are the factors affecting photoredox reaction pathways when both oxidative and reductive quenching seems equally feasible?

To address such questions, herein we employ porphyrins as photocatalysts where varying substituents and the state of metalation allows for adjusting their electrochemical potentials over ranges exceeding half a volt. These drastic changes in the redox properties of the PCs do not alter by much the overall yields of the light-driven reaction of a quaternary pyridinium salt with an activated alkyne. The key step involves photocatalytic reduction of the pyridinium cation (Py^+). Our analysis reveals an interplay between two parallel mechanisms that allows electron-rich and electron-deficient photocatalysts to drive the same reaction to completion, i.e., transforming the same starting materials into the same product. That is, the reaction mechanism and pathways adjust to the electronic properties of a catalyst.

RESULTS AND DISCUSSION

Model Reaction. Deaminative alkynylation (DAA), a reaction of activated alkynes with Katritzky salts, involves reductive activation of Py^+ via a sequence of photocatalyst-mediated CT steps (Scheme 1).[31] The photogenerated pyridyl radical **A** releases an alkyl radical **B** essential for the alkylation of alkyne **2**. Subsequent elimination of a tosyl radical yields product **3**.

Preparative electrochemistry can, indeed, provide the means for reducing Py^+ and drive DAA without a PC, stoichiometric amounts of sacrificial electron donors or acceptors and light illumination. The required 100 s of mM of supporting electrolyte presents formidable challenges when isolating and purifying the product from electrochemical reaction mixtures. In contrast, the minute amounts of colored PC can readily be removed, which illustrates a key practical advantage of photocatalysis, employing visible light irradiation to selectively drive the reaction to completion.

Earlier mechanistic studies reveal that the prevalent pathway of the reaction involves photoinduced electron transfer (PET) from the excited PC* to Py^+.[31] A subsequent reduction of the formed radical cation $PC^{\bullet+}$ by a hole transfer (HT) to DIPEA, which acts as a sacrificial electron donor, closes the catalytic cycle, i.e., PET-HT Mechanism (Scheme 1). Nevertheless, we cannot exclude the possibility for initial oxidation of the sacrificial donor via photoinduced hole transfer (PHT) from the excited PC* leading to the radical anion, $PC^{\bullet-}$. In this scenario the generated highly reducing species transfers electron to Py^+ (ET), illustrating an alternative pathway involving PHT-ET Mechanism.

Scheme 1. Model Deaminative Alkynylation with Katritzky Salts and Plausible Mechanistic Pathways[a]

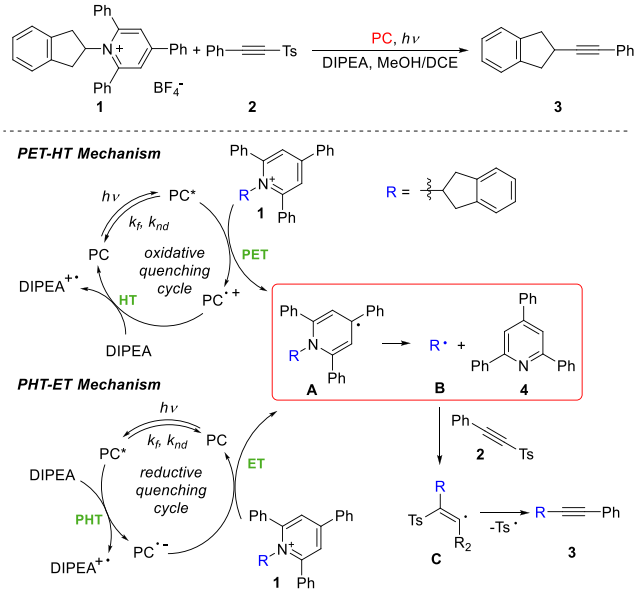

[a]Electron transfer (ET) is CT that involves a transduction of an electron to a lowest unoccupied molecular orbital (LUMO), HT is CT involving a transfer of an electron from a highest occupied molecular orbital (HOMO) to a singly occupied orbital, which is equivaled to moving a vacancy from a singly occupied orbital (i.e., the hole) to a higher lying HOMO.[32]

What defines the preference of the PET-HT (oxidative quenching) vs the PHT-ET (reductive quenching) pathways? Is it the interplay between the thermodynamic and kinetic control in regulating the preference for the reaction mechanism when parallel pathways are possible? The answers to these questions are important for designing and selecting PCs for light-driven redox transformations.

In the model DAA reaction, the photocatalyst drives the endergonic electron transfer from DIPEA to Py^+. The reduction potentials for oxidizing DIPEA and reducing Py^+ (**1**) are, respectively, $E^{(0)}_{DIPEA^{\bullet+}/DIPEA} = 0.86$ V vs SCE and $E^{(0)}_{Py^+/Py^\bullet} = -0.83$ V vs SCE for DCM in the presence of 0.1 M electrolyte. Thus, the optical excitation energy ($\mathcal{E}_{00}$) of a PC should overcome the hugely unfavorable driving force of this CT process, i.e.

$$\mathcal{E}_{00} > \Delta G_{CT}^{(0)} \approx F(E^{(0)}_{DIPEA^{\bullet+}/DIPEA} - E^{(0)}_{Py^+/Py^\bullet}) = 1.69\ \text{eV} \quad (1)$$

This "uphill" $\Delta G_{CT}^{(0)}$ corresponds to 735 nm near-infrared light radiation. Therefore, the bathochromic edge of the absorption spectrum of the photocatalyst should be in the visible spectral region, and many dyes meet this requirement. Furthermore, the reduction potentials of a PC for this reaction should bracket those of the pyridinium acceptor and of the sacrificial donor, i.e.

$$E^{(0)}_{PC/PC^{\bullet-}} < E^{(0)}_{Py^+/Py^\bullet} \quad (2a)$$

and

$$E^{(0)}_{PC^{\bullet+}/PC} > E^{(0)}_{DIPEA^{\bullet+}/DIPEA} \quad (2b)$$

https://dx.doi.org/10.1021/acscatal.0c00200
ACS Catal. 2020, 10, 5920−5927

The electrochemical and optical properties of tetraphenylporphyrin (**9**, Figure 1) should meet the requirements for photocatalyzing this DAA reaction.

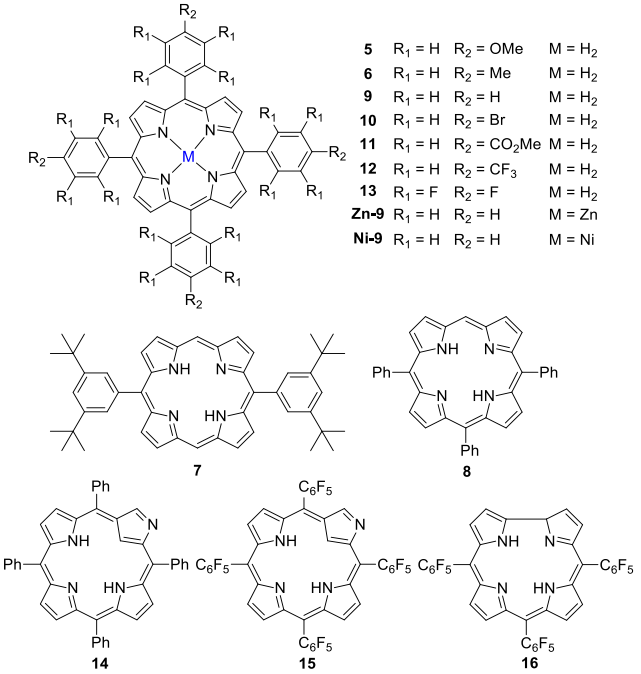

Figure 1. Porphyrinoids selected as photocatalysts for mechanistic studies.

The structure of porphyrin **9** provides a myriad of possibilities for attaining derivatives with a wide range of electronic properties via, for example, metalation or variation of substituents on the phenyls, R_1 and R_2. For mechanistic studies, therefore, we selected a series of porphyrinoids **5**-**16** taking under consideration their (1) commercial availability or straightforwardness of their synthesis, (2) solubility, and, above all, (3) diversity of their structural features and redox properties (Figure 1). While varying substituents at the periphery of the porphyrin macrocycle, along with incorporating different metal ions, does not truly alter the optical excitation energy $\mathcal{E}_{00}$, but it drastically changes the reduction potentials of oxidation between about 0.8 and 1.6 V vs SCE, and of reduction, between −1.3 and −0.7 V vs SCE (Table 1). As expected, porphyrins with electron-withdrawing substituents exhibit low reducing propensities, e.g., **12** and **13** while the electron-rich derivatives can act as strong reductants, e.g., **5** and **Zn-9**.

For porphyrinoids the electrochemical HOMO-LUMO gaps, $\mathcal{E}_{PC}$, are up to 400 meV larger than the optical HOMO-LUMO gaps, as represented by $\mathcal{E}_{00}$ (Table 1). It suggests considerable differences between the energies of the solvated ions and the photoexcited species as a corollary of favorable interactions between electrons and holes on spatially overlapping singly occupied molecular orbitals in the electronically excited states of the PCs.[34] These large differences between $\mathcal{E}_{00}$ and $\mathcal{E}_{PC}$, which can exceed the thermal energy at room temperature by more than an order of magnitude, i.e., for some of the PCs, $\mathcal{E}_{PC} - \mathcal{E}_{00} > 10k_BT$, illustrate the shortcomings of the oversimplified considerations for designing and selecting PCs (eqs 1 and 2). Specifically, even if eqs 1 and 2 are valid, the excited photocatalysts may not necessarily be good enough electron donors to reduce Py^+ or good enough electron acceptors to oxidize DIPEA. Hence, while eqs 1 and 2 represent necessary criteria, they are not sufficient for ensuring the feasibility of a PC for driving the desired chemical transformation.

Table 1. Electrochemical Potentials and Zero-to-Zero Excitation Energy of the Tested Photocatalysts

PC	$E^{(0)}_{PC/PC^{\bullet-}}$ [V][a]	$E^{(0)}_{PC^{\bullet+}/PC}$ [V][a]	$\mathcal{E}_{PC}$ [eV][b]	$\mathcal{E}_{00}$ [eV][c]	Φ_f	τ [ns]	yield of **3**[e,f] [%]
5	−1.24	0.91	2.15	1.90	0.065	8.12	59
6	−1.21	1.00	2.21	1.90	0.058	8.69	50
7	−1.17	1.06	2.23	1.96	0.042	10.5	54
8	−1.17	1.11	2.28	1.94	0.040	8.73	54
9	−1.20	1.04	2.24	1.91	0.048	8.31	55
10	−1.10	1.15	2.25	1.91	0.005	1.48	49
11	−1.05	1.21	2.26	1.91	0.037	8.88	53
12	−1.06	1.23	2.29	1.92	0.052	9.58	64
13	−0.74	1.63	2.37	1.94	0.021	10.20	66
Zn-9	−1.34	0.78	2.12	2.10	0.033	1.950	68
Ni-9	−1.24	1.11	2.35	1.90	0.010	8.76	56
14	−0.93[d]	0.96[d]	1.89	1.71	0.003	1.61	8
15	−1.19[d]	1.06[d]	2.25	1.73	0.001	0.64	9
16	−1.00[d]	1.10[d]	2.10	2.00	0.064	4.75	9

[a]From cyclic voltammetry measurements for DCM in the presence of 100 mM $(n\text{-}C_4H_9)_4NClO_4$, vs SCE. [b]Electrochemical HOMO−LUMO gap, $\mathcal{E}_{PC} \approx F(E^{(0)}_{PC^{\bullet+}/PC} - E^{(0)}_{PC/PC^{\bullet-}})$, where F is the Faraday constant. [c]From steady-state optical absorption and emission spectra for DCM. [d]From the inflection point of voltammogramic waves showing irreversible behavior.[33] [e]Reaction conditions: alkyne **2** (0.10 mmol), pyridinium salt **1** (1.4 equiv), PC (0.1 mol %), DIPEA (3.25 equiv), MeOH/DCE (c = 0.033 M), 2:1 volume ratio that corresponds to molar ratio, χ_{DCE} = 0.2, ambient temperature (20−22 °C), 16 h, under Ar atmosphere, light source: green LED diode (for more details see the SI). [f]GC yield.

Employing reaction conditions for **DAA** of pyridinium salt **1** with alkynyl *p*-tolylsulfone **2** that we previously established[31] reveals that all selected porphyrins exhibit good catalytic activity in a mixture of MeOH and DCE (Table 1). The use of chlorinated solvents ensure solubilization of the selected porphyrinoids **5** to **16** along with **Zn-9** and **Ni-9**, while polar protic media is essential for the progress of the reaction. Conversely, the *N*-confused porphyrins **14** and **15** and corrole **16**, do not prove truly efficient in catalyzing the model reaction, which we attribute to the lack of chemical reversibility of their electrochemical reduction and oxidation (see SI).[33,35] After the initial PCT, therefore side reactions, such as degradation of radical ions of porphyrins **14**−**16**, compete with the second CT steps essential for the PC recovery. This finding points to another important requirement for a photoredox catalyst: it has to exhibit reversible electrochemical oxidation and reduction behavior. Irreversibility of the voltammograms, however, does not necessarily render the PC unfeasible as the time scales of the electrochemical measurements employing slow to moderate scan rates tend to be orders of magnitude longer that the time constants of the CT steps, especially at high substrate loading.

Mechanistic Considerations. The DAA reaction can follow two distinctive pathways, PET-HT and PHT-ET, depending on the catalyst used. Cyclic voltammetry suggests that the generated pyridyl radical **A** is pronouncedly stable. In DCM the electrochemical reduction of Py^+ shows practically

https://dx.doi.org/10.1021/acscatal.0c00200
ACS Catal. 2020, 10, 5920−5927

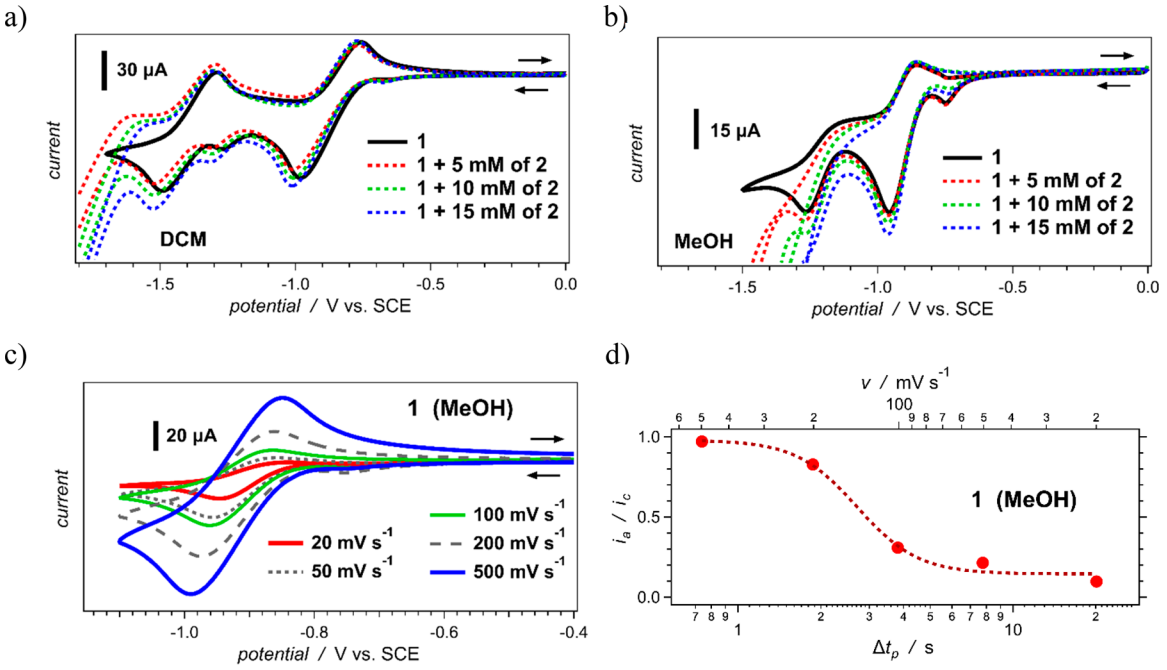

Figure 2. Electrochemical behavior of pyridinium salt **1**. (a and b) Cyclic voltammograms of **1** in the presence of various amounts of the alkyne **2** for DCM and MeOH recorded at a scan rate, ν = 100 mV s^{-1}. (c) Cyclic voltammograms of salt **1** for MeOH at different scan rates. (d) Dependence of the ratio between the anodic, i_a, and the cathodic, i_c, peaks (from c) on the scan rate and on the time delay between the two peaks, Δt_p, showing loss of reversibility when Δt_p exceeds about 2 s. All voltammograms are recorded in the presence of 100 mM N(*n*-Bu)$_4$ClO$_4$.

complete chemical reversibility at moderate scan rates (Figure 2). Conversely, MeOH induces a loss in the reversible behavior, which is consistent with fragmentation of pyridyl radical **A** to alkyl radical **B** and pyridine **4** occurring in time scales of seconds. Radical-trapping studies confirm the formation of intermediate **B** (see SI). These results concur with a sequential formation of intermediates **B**, **C**, and product **3**.

While the radical release, leading to product **3**, occurs in seconds, the PCT time scales are in the nanosecond and subnanosecond time domains. That is, the rates of PET and PHT have to be comparable or larger than the rates of radiative and nonradiative deactivation of the electronically excited states of the PCs. Therefore, considering the thermodynamics of the different CT steps, i.e., ensuring that $\Delta G^{(0)} < 0$, suffices as guidelines for selecting the PCs for this reaction.

The excited-state lifetimes (τ) of almost all porphyrins range between about 8 and 11 ns (Table 1), which appear to be long enough for the PCT steps that drive the chemical transformations. Even reactions catalyzed by porphyrins **10** and **Zn-9** with relatively short lifetimes (Table 1) give yields that are quite comparable to those from the other PCs. These findings strongly suggest that in this case the quantum yields of the PCT steps are not the limiting factor for obtaining the large overall reaction yields that we observe.

Conversely, the substituent-induced broad variation of the electrochemical properties of the porphyrins reveals underlying complexity of the mechanistic scenarios and an interplay of alternative pathways. An increase in the electron-withdrawing strength of the substituents, for example, should make a PC electron-deficient enough to completely shut down the initial PET with Py^+ and make the PET-HT mechanism impossible. Nevertheless, the electron-deficient tetra(pentafluorophenyl) porphyrin (**13**) is as effective PC as the electron-rich porphyrin **5**. The insufficiently negative reduction potentials of catalyst **13** (Table 1) indicate that it is not a good enough electron donor to photoreduce Py^+, which renders the PET-HT mechanism implausible. An alternative pathway in which strongly reducing radical anion $PC^{\bullet-}$ is generated, however, involving the PHT-ET mechanism (Scheme 1), can lead to the observed high yields of the reaction catalyzed by porphyrin **13**.

Upon photoexcitation of the PC in the reaction mixture, PET and PHT are the two competing initial steps that determine the pathway along which the reaction will progress. Therefore, we employ Stern−Volmer (SV) analysis for estimating the preference for PET-HT and PHT-ET mechanisms for each of the PCs. While using pyridinium salt **1** as a quencher allows for quantifying the bimolecular PET rate constants, quenching studies with DIPEA provide information about the PHT rate constants.

Many of the porphyrin derivatives are inherently electron rich with $\mathcal{E}_{00} < \mathcal{E}_{PC}$ (Table 1), and they do not manifest detectable quenching of their emission by DIPEA (Table 2 and Figure 3), which precludes the PHT-ET pathway as a possibility for these PCs. Furthermore, when $k_{q(DIPEA)} \ll k_{q(1)}$ (e.g., porphyrin **9** in MeOH and **Zn-9** in DCE), it suggests that the PET-HT mechanism dominates and PHT-ET has a minor contribution to the overall yields of the reaction driven by such electron-rich PCs. In contrast, while DIPEA quenches the emission of electron-deficient PCs, such as porphyrin **13**, salt **1** does not. Therefore, for such PCs the PHT-ET mechanism represents the only pathway toward the final product **3**.

For most PCs, the obtained values of k_q range between about 2 × 10^8 and 5 × 10^9 M^{-1} s^{-1}, which is typical for efficient bimolecular processes. For complex **Zn-9**, however, $k_{q(1)} > 1 \times 10^{10}$ M^{-1} s^{-1}, which exceeds the diffusion limits for biomolecular reactions in condensed phase and suggests for ground-state aggregation between the zinc porphyrin and Py^+.

https://dx.doi.org/10.1021/acscatal.0c00200
ACS Catal. 2020, 10, 5920−5927

Table 2. Emission-Quenching Results for Porphyrins Measured in DCE and MeOH

PC	solvent	$k_{q(DIPEA)}$ [$\times 10^8$ s^{-1} M^{-1}][a]	$k_{q(1)}$ [$\times 10^8$ s^{-1} M^{-1}][a]
5	DCE	[b]	24.5 ± 0.50
6	DCE	[b]	20.6 ± 0.70
7	DCE	[b]	19.4 ± 0.50
8	DCE	[b]	15.2 ± 0.70
9	DCE	[b]	8.06 ± 0.71
9	MeOH[c]	4.68 ± 0.31	26.8 ± 1.8
10	DCE	[b]	36.6 ± 0.40
11	DCE	3.29 ± 0.11	4.01 ± 0.23
12	DCE	6.63 ± 0.17	8.97 ± 0.18
12	MeOH[c]	9.15 ± 0.2	3.72 ± 0.22
13	DCE	41.1 ± 0.2	[b]
13	MeOH[c]	50.0 ± 0.6	[b]
Zn-9	DCE	25.2 ± 3.2	376 ± 11
Zn-9	MeOH[c]	[b]	161 ± 28
Ni-9	DCE	[b]	23.0 ± 1.1

[a]Emission-quenching rate constants, k_q, for DIPEA and salt **1** obtained from the SV analysis. [b]Emission quenching is not detected. [c]In the presence of either only salt **1** or only DIPEA, all PCs, except porphyrins **9**, **12**, **13**, and **Zn-9**, exhibit instability in MeOH media. Therefore, we employ DCE for the SV analysis and for porphyrins **9**, **12**, **13**, and **Zn-9**, for others we also use MeOH.

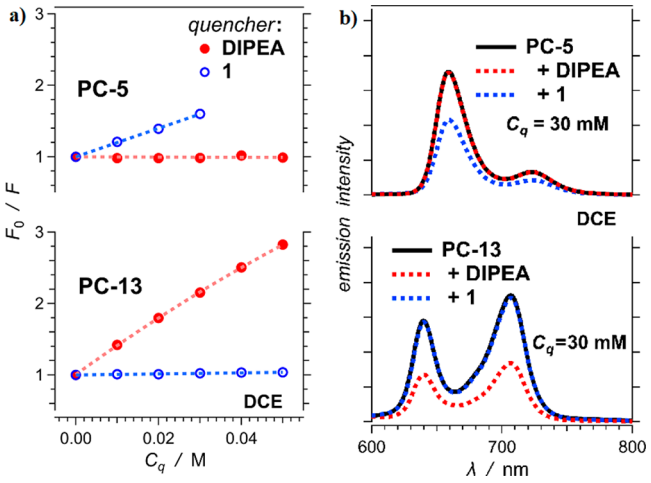

Figure 3. Stern–Volmer (SV) analysis for electron-rich and electron-deficient PCs **5** and **13**, respectively, obtained from optical spectra recorded for DCE. (λ_{ex} = 518 and 506 nm for **5** and **13**, respectively.)

The electronic properties of the PCs correlate well with the outcomes from the SV studies that reveal the preferred pathways for the light-driven formation of radicals. As informative as the SV analysis is about the parallel mechanisms at play, it can examine only the plausibility and the nature of the initial PCT steps.

Charge-Transfer Analysis. Evaluation of the thermodynamic driving forces, $-\Delta G^{(0)}$, of the different CT steps involved is essential for analyzing the feasibility and the interplay between the PET-HT and PHT-ET mechanisms:[36,37]

PET-HT mechanism: oxidative quenching

PET: $PC^* + Py^+ \rightarrow PC^{\bullet+} + Py^{\bullet}$

$$\Delta G^{(0)}_{PET} = F(E^{(0)}_{PC/PC^{\bullet+}} - E^{(0)}_{Py^+/Py^{\bullet}}) - \mathcal{E}_{00} + \Delta G_S + W \quad (3a)$$

HT: $PC^{\bullet+} + DIPEA \rightarrow PC + DIPEA^{\bullet+}$

$$\Delta G^{(0)}_{HT} = F(E^{(0)}_{DIPEA/DIPEA^{\bullet+}} - E^{(0)}_{PC^{\bullet+}/PC}) + \Delta G_S + W \quad (3b)$$

PHT-ET mechanism: reductive quenching

PHT: $PC^* + DIPEA \rightarrow PC^{\bullet-} + DIPEA^{\bullet+}$

$$\Delta G^{(0)}_{PHT} = F(E^{(0)}_{DIPEA^{\bullet+}/DIPEA} - E^{(0)}_{PC/PC^{\bullet-}}) - \mathcal{E}_{00} + \Delta G_S + W \quad (3c)$$

ET: $PC^{\bullet-} + Py^+ \rightarrow PC + Py^{\bullet}$

$$\Delta G^{(0)}_{ET} = F(E^{(0)}_{PC/PC^{\bullet-}} - E^{(0)}_{Py^+/Py^{\bullet}}) + \Delta G_S + W \quad (3d)$$

where ΔG_S is the Born solvation energy and W is the Coulomb work term.[36] The frequently used excited-state electrochemical potentials of PCs, obtained from differences between their ground-state reduction potentials and $\mathcal{E}_{00}$, do not account for W, which depends on the donor and the acceptor rather than only on the photocatalyst.

For the electron-rich complex **Zn-9**, $\Delta G_{PET}^{(0)}$ assumes large negative values, while the large positive estimates of $\Delta G_{PET}^{(0)}$ are apparent for the electron deficient porphyrin **13** (Figure 4a). These findings concur perfectly with the SV results.

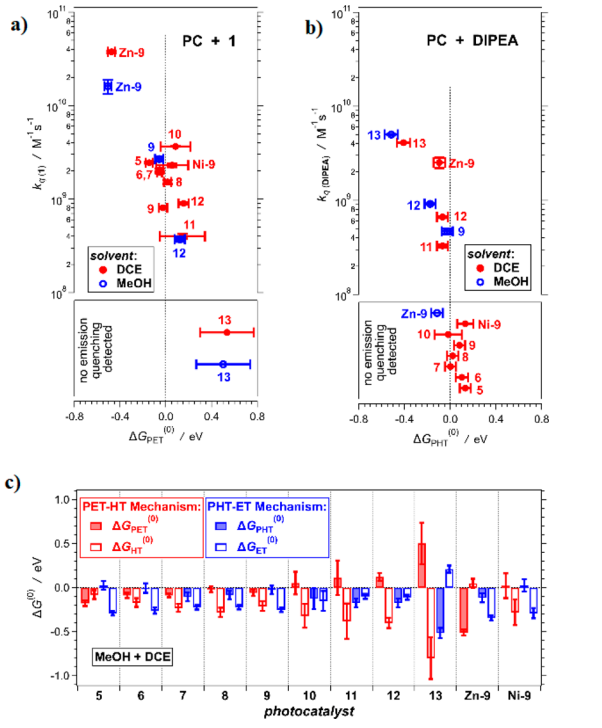

Figure 4. (a and b) Correlation between the emission-quenching rate constants (obtained from the SV analyses) and the driving forces for the photoinduced charge transfer steps (estimated using eq 3) for DCE and MeOH. (c) Driving forces for the CT steps involving the different photocatalysts as estimated using eq 3 for MeOH/DCE mixture, χ_{DCE} = 0.2.

Conversely, salt **1** quenches the emission of all PCs for which the estimated values of $\Delta G_{PET}^{(0)}$ cluster around zero, i.e., -0.15 eV $\leq \Delta G_{PET}^{(0)} \leq 0.15$ eV. While small driving forces do not preclude efficient CT,[38−40] the quenching of the emission of the relatively electron-deficient PCs, such as porphyrin **12**, appears counterintuitive. That is, the $\Delta G_{PET}^{(0)}$ estimate for catalyst **12** corresponds to about $6\times k_BT$, which is substantial

https://dx.doi.org/10.1021/acscatal.0c00200
ACS Catal. 2020, 10, 5920−5927

and should prevent the PET step from occurring, but it does not.

Conversely, the estimates for $\Delta G_{PHT}^{(0)}$ correlate truly well with the emission quenching behavior with DIPEA, and shows opposite trends in comparison to that with salt **1**. As expected, for the electron deficient porphyrin **13**, $\Delta G_{PHT}^{(0)}$ assumes large negative values, reaching $-20\times k_BT$, and DIPEA efficiently quenches its emission (Figure 3). DIPEA also quenches the emission of the PCs with small **PHT** driving forces, i.e., -0.18 eV $\leq \Delta G_{PHT}^{(0)} \leq -0.03$ eV. Concurrently, it does not perturb the emission of the PCs with small positive estimates for $\Delta G_{PHT}^{(0)}$, i.e., -0.02 eV $\leq \Delta G_{PHT}^{(0)} \leq 0.13$ eV (Figure 4b). These results illustrates a tight correlation between the experimentally obtained $k_{q(DIPEA)}$ and the calculated $\Delta G_{PHT}^{(0)}$; something that we do not quite observe for $k_{q(1)}$ and $\Delta G_{PET}^{(0)}$.

The values of $\Delta G_{PET}^{(0)}$ and $\Delta G_{PHT}^{(0)}$, along with the SV analysis, reveal which pathway, PET-HT or PHT-ET, prevails. For operational PET-HT mechanism, however, $\Delta G_{PET}^{(0)}$ and $\Delta G_{HT}^{(0)}$ should assume negative values (eq 3). If $\Delta G_{PET}^{(0)} < 0$ and $\Delta G_{HT}^{(0)} > 0$, the SV analysis would still reveal emission quenching with salt **1**, but the **DAA** reaction would not proceed with detectable yields. Nonoperational HT causes buildup of PET-generated $PC^{\bullet+}$ and prevents the turnover of the catalyst. In a similar manner, $\Delta G_{PHT}^{(0)}$ and $\Delta G_{ET}^{(0)}$ should assume negative values for operational PHT-ET mechanism, because $\Delta G_{PHT}^{(0)} < 0$ and $\Delta G_{ET}^{(0)} > 0$ will lead to buildup of PHT-generated $PC^{\bullet-}$.

For the selected porphyrins $\mathcal{E}_{00} < \mathcal{E}_{PC}$, which indicates that $\Delta G_{ET}^{(0)} < 0$ if $\Delta G_{PET}^{(0)} \lesssim 0$, and $\Delta G_{HT}^{(0)} < 0$ if $\Delta G_{PHT}^{(0)} \lesssim 0$ (Figure 4 a,b). The very good DAA reaction yields are clear evidence that for all porphyrin PCs in this study the HT and ET steps will occur after the initial PET and PHT, respectively (Figure 4c). Nevertheless, while porphyrin **13** shows $\Delta G_{ET}^{(0)} > 0$ (Figure 4c), it catalyzes the reaction efficiently via PHT-ET mechanism as the SV analysis and the estimated $\Delta G_{PCT}^{(0)}$ values indicate.

These discrepancies of efficient quenching by salt **1** and high reaction yields when $\Delta G_{PET}^{(0)} > 0$ and $\Delta G_{ET}^{(0)} > 0$, respectively, point to two important consideration about the interpretation of the thermodynamic results from eq 3. (1) The electrochemical potentials are extracted from data for samples with large amounts of supporting electrolyte inducing ion pairing.[41] It may affect the results for charged species, such as Py^+, sufficiently enough to produce unfavorable PET and ET driving forces (eq 3) that do not necessarily reflect the thermodynamics for in the absence of electrolyte (see the SI). (2) For bimolecular reactions, the lack of precise information about the donor–acceptor distances during the CT steps can lead to sufficient uncertainties in the estimations of W, and thus, of $\Delta G^{(0)}$ (eq 3).

The outcomes for the most electron-rich porphyrins, **Zn-9**, provide important examples in pertinence to these considerations. While an increase in the solvent polarity causes a small negative shift in $\Delta G_{PHT}^{(0)}$, the SV analysis reveals that DIPEA quenches the **Zn-9** emission in DCE but not in MeOH (Table 2 and Figure 4b). Changing from DCE to MeOH increases the reorganization energy by about 0.2 eV, which places the PHT kinetics for this solvent further from the tip of the Marcus curve. This trend, indeed, induces a decrease in the rates of PHT for MeOH, but not to an extent where the quenching of the **Zn-9** emission by DIPEA is not detectable at all. Conversely, the optical absorption spectra of **Zn-9** show ground-state aggregation in the presence of DIPEA for DCE but not for MeOH (Figure 5). Concurrently, **Zn-9** aggregates with Py^+ in both solvents (see the SI).

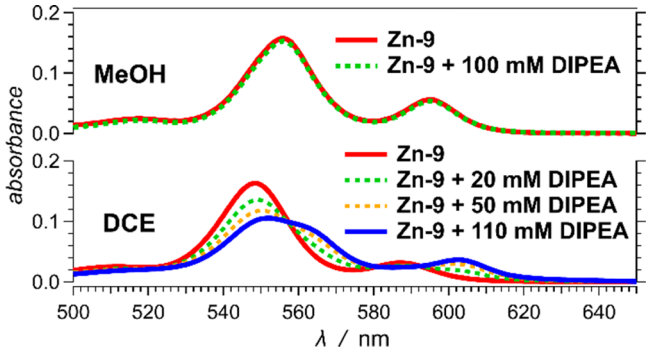

Figure 5. Solvent effects of the optical absorption spectra focused on the Q-bands of **Zn-9** (5.8×10^{-6} M) in the presence of various amounts of DIPEA.

These binding trends are consistent with the outcomes from the SV analysis and point to another important feature of photoredox catalysis. More often than never, dynamic collisional pathways may not provide a long enough residence time of the photoexcited PC and the substrate in proximity to each other, and sufficiently strong donor–acceptor electronic coupling, to ensure efficient PCT. Regardless how favorable the driving forces are (eq 3), a sufficient donor–acceptor electronic coupling is essential for each of the CT steps to occur, and bimolecular dynamics adds to this challenge. Alternatively, static mechanisms, where the PC-substrate binding prior to PCT is stronger than the PC-product binding after it, illustrate an important bioinspired approach for catalyst design.

The outcomes of the thermodynamic CT analysis (Figure 4) illustrate the multifaceted complexity of driving multistep endergonic electron transfer from the sacrificial donor to the substrate. Favorable driving forces for all steps are indeed a necessary, but not a sufficient condition. Collectively, the outcomes from the thermodynamic CT calculations (eq 3), the SV studies (Table 2 and Figure 3), and trends in the optical spectra (Figure 5) unveil crucial mechanistic details that neither of these individual analyses can readily predict on its own.

CONCLUSIONS

Photochemical reactions provide a broad access to products that are impossible to obtain by any other means and they are extremely sensitive to the match between the electronic properties of the photocatalysts and the substrates. The presented example shows that the mechanism of light-driven deaminative alkynylation adjusts to the electrochemical properties of the dyes, in this case porphyrins. That is, electron-rich and electron-deficient porphyrins drive the same reaction with similar efficiencies via different CT routes involving oxidative versus reductive quenching; specifically, the substrate extracts an electron from the photoexcited or singly reduced catalyst, i.e., PC* or $PC^{\bullet-}$ (Scheme 1), depending on the thermodynamic feasibility of the steps in each of the pathways. Furthermore, our results indicate that the rational selection of photoredox catalysts should involve multifaceted analyses focusing not only on the electrochemical potentials

https://dx.doi.org/10.1021/acscatal.0c00200
ACS Catal. 2020, 10, 5920–5927

and the optical excitation energies, but also on the nature of the collision complexes in bimolecular interactions. In addition to favorable driving forces, sufficient donor−acceptor coupling is crucial for ensuring CT rates large enough to compete with the dissociation of the CT complexes, for driving the chemical transformations with acceptable yields.

■ ASSOCIATED CONTENT

Supporting Information

The Supporting Information is available free of charge at https://pubs.acs.org/doi/10.1021/acscatal.0c00200.

Experimental procedures, photocatalytic and electrochemical studies, Stern−Volmer analysis, and calculations of charge-transfer driving forces (PDF)

■ AUTHOR INFORMATION

Corresponding Authors

Dorota Gryko − *Institute of Organic Chemistry Polish Academy of Sciences, 01-224 Warsaw, Poland;* orcid.org/0000-0002-5197-4222; Email: dorota.gryko@icho.edu.pl; http://ww2.icho.edu.pl/gryko_group

Valentine I. Vullev − *Department of Bioengineering and Department of Chemistry, Department of Biochemistry, and Materials Science and Engineering Program, University of California at Riverside, Riverside, California 92521, United States;* orcid.org/0000-0002-3416-9686; Email: vullev@ucr.edu

Authors

Katarzyna Goliszewska − *Institute of Organic Chemistry Polish Academy of Sciences, 01-224 Warsaw, Poland*

Katarzyna Rybicka-Jasińska − *Institute of Organic Chemistry Polish Academy of Sciences, 01-224 Warsaw, Poland*

John A. Clark − *Department of Bioengineering, University of California at Riverside, Riverside, California 92521, United States*

Complete contact information is available at: https://pubs.acs.org/10.1021/acscatal.0c00200

Notes

The authors declare no competing financial interest.

■ ACKNOWLEDGMENTS

Financial support for this work was provided by the Foundation for Polish Sciences (FNP TEAM POIR.04.04.00-00-4232/17-00), the National Science Center (PL) KRJ Etiuda, UMO-2017/24/T/ST5/00032, and the U.S.A. National Science Foundation (Grants CHE 1800602 and CHE 1465284, along with an AGEP supplement for J.A.C.). V.I.V. thanks the Fulbright Commission Brazil, and the authors extend their gratitude to Dr. Maksymilian Karczewski and Dr. Eli M. Espinoza for computing the radii of the redox species used for this work.

■ REFERENCES

(1) Braslavsky, S. E. Glossary of terms used in photochemistry, 3rd edition (IUPAC Recommendations 2006). *Pure Appl. Chem.* **2007**, *79*, 293−465.

(2) Bard, A. J.; Memming, R.; Miller, B. Terminology in semiconductor electrochemistry and photoelectrochemical energy conversion (Recommendations 1991). *Pure Appl. Chem.* **1991**, *63*, 569−596.

(3) Osterloh, F. E. Photocatalysis versus Photosynthesis: A Sensitivity Analysis of Devices for Solar Energy Conversion and Chemical Transformations. *ACS Energy Lett.* **2017**, *2*, 445−453.

(4) Romero, N. A.; Nicewicz, D. A. Organic Photoredox Catalysis. *Chem. Rev.* **2016**, *116*, 10075−10166.

(5) Prier, C. K.; Rankic, D. A.; MacMillan, D. W. C. Visible Light Photoredox Catalysis with Transition Metal Complexes: Applications in Organic Synthesis. *Chem. Rev.* **2013**, *113*, 5322−5363.

(6) Zhang, X.; Rakesh, K. P.; Ravindar, L.; Qin, H. L. Visible-light initiated aerobic oxidations: A critical review. *Green Chem.* **2018**, *20*, 4790−4803.

(7) Michelin, C.; Hoffmann, N. Photocatalysis applied to organic synthesis − A green chemistry approach. *Curr. Opin. Green Sustain. Chem.* **2018**, *10*, 40−45.

(8) Reckenthäler, M.; Griesbeck, A. G. Photoredox catalysis for organic syntheses. *Adv. Synth. Catal.* **2013**, *355*, 2727−2744.

(9) Ghosh, T.; Slanina, T.; König, B. Visible light photocatalytic reduction of aldehydes by Rh(III)-H: A detailed mechanistic study. *Chem. Sci.* **2015**, *6*, 2027−2034.

(10) Xie, J.; Jin, H.; Hashmi, A. S. K. The recent achievements of redox-neutral radical C-C cross-coupling enabled by visible-light. *Chem. Soc. Rev.* **2017**, *46*, 5193−5203.

(11) Wang, C. S.; Dixneuf, P. H.; Soulé, J. F. Photoredox Catalysis for Building C-C Bonds from C(sp2)-H Bonds. *Chem. Rev.* **2018**, *118*, 7532−7585.

(12) Fagnoni, M.; Dondi, D.; Ravelli, D.; Albini, A. Photocatalysis for the Formation of the C−C Bond. *Chem. Rev.* **2007**, *107*, 2725−2756.

(13) Zhu, J.; Yang, W. C.; Wang, X. D.; Wu, L. Photoredox Catalysis in C−S Bond Construction: Recent Progress in Photo-Catalyzed Formation of Sulfones and Sulfoxides. *Adv. Synth. Catal.* **2018**, *360*, 386−400.

(14) Zhao, Y.; Xia, W. Recent advances in radical-based C-N bond formation: Via photo-/electrochemistry. *Chem. Soc. Rev.* **2018**, *47*, 2591−2608.

(15) Revathi, L.; Ravindar, L.; Fang, W. Y.; Rakesh, K. P.; Qin, H. L. Visible Light-Induced C−H Bond Functionalization: A Critical Review. *Adv. Synth. Catal.* **2018**, *360*, 4652−4698.

(16) Qin, Q.; Jiang, H.; Hu, Z.; Ren, D.; Yu, S. Functionalization of C-H Bonds by Photoredox Catalysis. *Chem. Rec.* **2017**, *17*, 754−774.

(17) König, B. Photocatalysis in Organic Synthesis − Past, Present, and Future. *Eur. J. Org. Chem.* **2017**, *2017*, 1979−1981.

(18) Ghosh, I.; Bardagi, J. I.; König, B. Reply to 'Photoredox Catalysis: The Need to Elucidate the Photochemical Mechanism'. *Angew. Chem., Int. Ed.* **2017**, *56*, 12822−12824.

(19) Buzzetti, L.; Crisenza, G. E. M.; Melchiorre, P. Mechanistic Studies in Photocatalysis. *Angew. Chem., Int. Ed.* **2019**, *58*, 3730−3747.

(20) Arias-Rotondo, D. M.; McCusker, J. K. The photophysics of photoredox catalysis: A roadmap for catalyst design. *Chem. Soc. Rev.* **2016**, *45*, 5803−5820.

(21) Nacsa, E. D.; MacMillan, D. W. C. Spin-Center Shift-Enabled Direct Enantioselective α-Benzylation of Aldehydes with Alcohols. *J. Am. Chem. Soc.* **2018**, *140*, 3322−3330.

(22) Singh, A.; Teegardin, K.; Kelly, M.; Prasad, K. S.; Krishnan, S.; Weaver, J. D. Facile synthesis and complete characterization of homoleptic and heteroleptic cyclometalated Iridium(III) complexes for photocatalysis. *J. Organomet. Chem.* **2015**, *776*, 51−59.

(23) Speckmeier, E.; Fischer, T. G.; Zeitler, K. A Toolbox Approach To Construct Broadly Applicable Metal-Free Catalysts for Photoredox Chemistry: Deliberate Tuning of Redox Potentials and Importance of Halogens in Donor-Acceptor Cyanoarenes. *J. Am. Chem. Soc.* **2018**, *140*, 15353−15365.

(24) McCarthy, B. G.; Pearson, R. M.; Lim, C.-H.; Sartor, S. M.; Damrauer, N. H.; Miyake, G. M. Structure-property relationships for tailoring phenoxazines as reducing photoredox catalysts. *J. Am. Chem. Soc.* **2018**, *140*, 5088−5101.

(25) Joshi-Pangu, A.; Lévesque, F.; Roth, H. G.; Oliver, S. F.; Campeau, L. C.; Nicewicz, D.; DiRocco, D. A. Acridinium-Based

Photocatalysts: A Sustainable Option in Photoredox Catalysis. *J. Org. Chem.* **2016**, *81*, 7244−7249.
(26) Nguyen, J. D.; Tucker, J. W.; Konieczynska, M. D.; Stephenson, C. R. J. Intermolecular Atom Transfer Radical Addition to Olefins Mediated by Oxidative Quenching of Photoredox Catalysts. *J. Am. Chem. Soc.* **2011**, *133*, 4160−4163.
(27) Wallentin, C.-J.; Nguyen, J. D.; Finkbeiner, P.; Stephenson, C. R. J. Visible Light-Mediated Atom Transfer Radical Addition via Oxidative and Reductive Quenching of Photocatalysts. *J. Am. Chem. Soc.* **2012**, *134*, 8875−8884.
(28) For examples of oxidative quenching see: (a) Tlahuext-Aca, A.; Garza-Sanchez, R. A.; Glorius, F. Multicomponent Oxyalkylation of Styrenes Enabled by Hydrogen-Bond-Assisted Photoinduced Electron Transfer. *Angew. Chem., Int. Ed.* **2017**, *56*, 3708−3711. (b) Kong, W.; Yu, C.; An, H.; Song, Q. Photoredox-Catalyzed Decarboxylative Alkylation of Silyl Enol Ethers To Synthesize Functionalized Aryl Alkyl Ketones. *Org. Lett.* **2018**, *20*, 349−352. (c) Cheng, W.-M.; Shang, R.; Fu, Y. Photoredox/Brønsted Acid Co-Catalysis Enabling Decarboxylative Coupling of Amino Acid and Peptide Redox-Active Esters with *N*-Heteroarenes. *ACS Catal.* **2017**, *7*, 907−911.
(29) For examples of reductive quenching see: (a) Okada, K.; Okamoto, K.; Morita, N.; Okubo, K.; Oda, M. Photosensitized decarboxylative Michael addition through N-(acyloxy)phthalimides via an electron-transfer mechanism. *J. Am. Chem. Soc.* **1991**, *113*, 9401−9402. (b) Yang, J.; Zhang, J.; Qi, L.; Hu, C.; Chen, Y. Visible-light-induced chemoselective reductive decarboxylative alkynylation under biomolecule-compatible conditions. *Chem. Commun.* **2015**, *51*, 5275−5278. (c) Xu, K.; Tan, Z.; Zhang, H.; Liu, J.; Zhang, S.; Wang, S. Photoredox catalysis enabled alkylation of alkenyl carboxylic acids with *N*-(acyloxy)phthalimide via dual decarboxylation. *Chem. Commun.* **2017**, *53*, 10719−10722.
(30) Mei, M.; Anand, D.; Zhou, L. Divergent Conversion of *N*-Acyl-isoxazol-5(2H)-ones to Oxazolesand 1,3-Oxazin-6-ones Using Photoredox Catalysis. *Org. Lett.* **2019**, *21*, 3548−3553.
(31) Ociepa, M.; Turkowska, J.; Gryko, D. Redox-Activated Amines in C(sp^3)−C(sp) and C(sp^3)−C(sp^2) Bond Formation Enabled by Metal-Free Photoredox Catalysis. *ACS Catal.* **2018**, *8*, 11362−11367.
(32) Derr, J. B.; Tamayo, J.; Espinoza, E. M.; Clark, J. A.; Vullev, V. I. Dipole-induced effects on charge transfer and charge transport. Why do molecular electrets matter? *Can. J. Chem.* **2018**, *96*, 843−858.
(33) Espinoza, E. M.; Clark, J. A.; Soliman, J.; Derr, J. B.; Morales, M.; Vullev, V. I. Practical Aspects of Cyclic Voltammetry: How to Estimate Reduction Potentials When Irreversibility Prevails. *J. Electrochem. Soc.* **2019**, *166*, H3175−H3187.
(34) Uno, B.; Okumura, N. Molecular Scientific Approach in Electroorganic Chemistry. *Recent Res. Dev. Pure Appl. Chem. 2* **1998**, 83−99.
(35) Espinoza, E. M.; Larsen, J. M.; Vullev, V. I. What Makes Oxidized N-Acylanthranilamides Stable? *J. Phys. Chem. Lett.* **2016**, *7*, 758−764.
(36) Bao, D.; Millare, B.; Xia, W.; Steyer, B. G.; Gerasimenko, A. A.; Ferreira, A.; Contreras, A.; Vullev, V. I. Electrochemical oxidation of ferrocene: A strong dependence on the concentration of the supporting electrolyte for nonpolar solvents. *J. Phys. Chem. A* **2009**, *113*, 1259−1267.
(37) Rehm, D.; Weller, A. Kinetics of fluorescence quenching by electron and H-atom transfer. *Isr. J. Chem.* **1970**, *8*, 259−271.
(38) Purc, A.; Espinoza, E. M.; Nazir, R.; Romero, J. J.; Skonieczny, K.; Jeżewski, A.; Larsen, J. M.; Gryko, D. T.; Vullev, V. I. Gating That Suppresses Charge Recombination-The Role of Mono-*N*-Arylated Diketopyrrolopyrrole. *J. Am. Chem. Soc.* **2016**, *138*, 12826−12832.
(39) Bao, D.; Upadhyayula, S.; Larsen, J. M.; Xia, B.; Georgieva, B.; Nuñez, V.; Espinoza, E. M.; Hartman, J. D.; Wurch, M.; Chang, A.; Lin, C.-K.; Larkin, J.; Vasquez, K.; Beran, G. J. O.; Vullev, V. I. Dipole-Mediated Rectification of Intramolecular Photoinduced Charge Separation and Charge Recombination. *J. Am. Chem. Soc.* **2014**, *136*, 12966−12973.
(40) Krzeszewski, M.; Espinoza, E. M.; Červinka, C.; Derr, J. B.; Clark, J. A.; Borchardt, D.; Beran, G. J. O.; Gryko, D. T.; Vullev, V. I. Dipole Effects on Electron Transfer are Enormous. *Angew. Chem., Int. Ed.* **2018**, *57*, 12365−12369.
(41) Bird, M. J.; Iyoda, T.; Bonura, N.; Bakalis, J.; Ledbetter, A. J.; Miller, J. R. Effects of electrolytes on redox potentials through ion pairing. *J. Electroanal. Chem.* **2017**, *804*, 107−115.

https://dx.doi.org/10.1021/acscatal.0c00200
ACS Catal. 2020, 10, 5920−5927